VOL. 18, NO. 19, OCTOBER 2023 ISSN 1819-6608
ARPN Journal of Engineering and Applied Sciences

www.arpnjournals.com

RECOGNIZING SURFACE EDGES AND PREDICTION OF TERRAIN DEFORMATION BYANALYZING LANDSAT-8 RASTER IN QGIS-A CASE STUDY OF COIMBATORE, INDIA

G. Shanthi, Prasanna B., Pooja A. C., Philip Galvin Mendez and Kowshikaa T.
Department of Electrical and Computer Engineering, Sri Krishna College of Technology, Coimbatore, Tamil Nadu, India
E-Mail: shanthi.g@skct.edu.in

ABSTRACT

Convolutional Neural Network (CNN) is one of the deep learning algorithms generally used for image recognition and allocation. These neural networks are developed in multi-layers which reasonably reduces complex dimensions of any input without ruining original information. The satellite images are obtained in .jpg format with potential resolutions. The land usage of the given area is estimated and the objects present in the image are identifiedusing the Canny Edge detection algorithm. It extracts useful data in terms of structures and scales down the size of the data. Raster data in.tif format from LANDSAT-8 is collected over a year. With the Semi-automated classification plugin (SCP) in QGIS, the signatures are created. Signatures are pixelated polygons that are classified to store land attributes. The Normalized indices of vegetation (NDVI), water (NDWI), and built-up (NDBI) are calculated. Land use land cover area was developed. Multi-layer perceptron has numerous hidden layers, and the iterations can be fixed in the MOLUSCE plugin. The land cover for two years, 2020 and 2023 is given along with spatial variables such as precipitation and elevation. The changes in each category of land are identified. In the last three years, the area covered by buildings has increased from 25% to 31%. The area under water bodies had a slight decrease from 1.46% to 1.25%. The land cover for the year 2026 is predicted. From the predictions, it is conclusive that, our research supports the changes between 3 years had not much difference, but above 6 years, it is evident thatland will be deformed from most of the vegetation area into built-up.

Keywords: CNN, land cover, raster, MLP, signatures, MOLUSCE, spatial, Coimbatore.

Manuscript Received 22 August 2023; Revised 15 November 2023; Published 11 December 2023

1. INTRODUCTION

The term "neural networks" is being used in every field of applications since they are responsible for classifying as many images. The magnitude of neural networks is reaching its peak. Building deep learning models for assigning tasks from simpler to increasingly complex levels has progressed and so gathered the attention of many researchers. The input layers take the necessary parameters to the hidden layer. The uncommon features are extracted through several continuous processes [1]. The overall performance matrices are dependent on the amount of training and testing images given to the neural network. Remote sensing will play an inevitable role in obtaining information about our region of interest (ROI). It carries rich data about monitoring, sensing, and recording events such as movements in theland surface, water bodies, climatic changes, natural hazards, and military activities [2]. In the digitized era, the integration of various kinds of data is necessary. Satellite imagery has unique resolutions and frequencies and the same will be suited for field-based cameras. Access to a large amount of data supports building machine learning models each giving rise to algorithms. For every application, the approaches for selecting the algorithm can vary. Supervised learning has the advantage of being labeled classes, and the number of hidden layers can be minimized for processing. However, the computational cost arises when the trained data is unlabeled and requires more hidden layers [3]. The CNNs are also employed in decision-making systems in superior industries where the objects are identified and classified for further mechanism. Making adjustments in the deep learning models can expand the interest in counting Computer Vision (CV).

The combined training methodologies have far better results [4]. Such examples are edge detection, tracing contours, framing the area covered by each object, applying thresholds for imaging analyses, and masking. The human brain can do severe complex vision-based classification, yet there is a valid reason why computer vision has so much demand over human vision. The machines are provided with immense storage of pre-defined data, along with the ability to capture meaningful pieces of information such as textures, shapes, and colors. Although these processes arereplicated in the human brain, the sensitivity of repeating assigned tasks is viable in computer vision alone. Computer vision still has a lot to learn from neuroscience [5].

Edge detection is the basic algorithm that traces out the boundaries of each object within the picture. They work by identifying changes in color intensities. Usually, color intensities drop on boundaries, which indicates an edge. Several algorithms based upon edge detectors are used, but the Canny edge detector is preferred best of all. It smoothens the image and applies a Gaussian kernel where high and low values can be drawn. This method is known for image segmentation, as the unimportantdata can be neglected. [6] The canny edge detector improves the model's quality to achieve the best results. The processing of additional white noise during edge detection is noticeable [8].

Thresholding is a process generally meant for noise cancellation from the edge detectors and makes edges clearer. Choosing the legitimate value of the threshold is always adopted. Loss of information can happen if the value is too high for edge detection. In binary thresholding, a single level of value is set. The set of values that are higher than the threshold is defined as one class, and values lower than the threshold are classified into another class. The variations in the image intensities are verysensitive. [12] Adaptive thresholding is more robust to variations in the intensities. The threshold value for each pixel is set by the neighboring pixel. The applications where the image is subjected to uniform lighting conditions use Adaptive thresholding. With the acute developments of machine learning and artificial intelligence, the process of pattern tracing and edge tracking can be made to detect automatically [10].

The satellite images are comprised of red, green, and blue pixels with additional channels for imaging. Each channel describes the saturation levels of pixels combined [11]. The raster data of satellites such as LANDSAT has several bands each consisting of separate operational ranges and frequencies. They are of 7 to 11 band combinations of blue, green, red, NIR, SWIR, and TIRS. The land cover map is created based on the band combinations of 5-4-3. Signatures are the "regions" that are assigned to carry classes of built-up, water, and vegetation areas by creating pixelpolygons. The semi-automatic classification plugin in QGIS provides a set of tools for raster processing such that it can automate the workflow. It has the amplitude to train the signatures of subsequent classes and develop the land cover map Variations in the land cover map are a direct indication of how the raster information is performed. The size of raster data is pretty large and it will be around 30 Mb for an area of 750 square kilometers. If the data is reduced below800 Kb, it will be efficient to accommodate more images and the processing time will be fast. For predicting land use and land cover, the records of past years should be taken as input.

The MOLUSCE plugin in QGIS makes the predictions by analyzing the land cover data and spatial variables such as elevation, and precipitation. Rapid industrialization causes the socioeconomic conditions of the state. Before 50-60 years ago, the globe was surrounded mostly by vegetation lands and unpolluted water bodies. Rapid evolution in machines and polluting artifacts have caused certain changes in external surroundings. More are more buildings are constructed, thereby displacing agricultural communities from their place to urban infrastructures. It leads to the fragmentation of natural habitats and can break the biodiversity chain. Forests are degraded from highly invaluable sources of vegetationto dry barren lands.

Global warming hurts global climate change. Since then, the annual rainfall has been declining. It's been difficult for climatologists to predict the unusual downpour over the past decade. Population density is advancing to new peaks. 2 billion were added just in the last 20 years. These shifts are compelling and havea major influence on the land cover changes. Despite these challenges, there are hopes to renovate the sustainable land cover. Conversion strategies such as agroforestry practices to increase the yields of crops and millet. Several spatial analysis and simulation methods can recollect and visualize the actual mechanisms that are responsible for land deformation.

Many studies have accepted that changes in LULC, especially urbanization, depletion of resources and forests, division of arable land, debased aquatic habitat, and increased carbon and heat production, all have contributed to the profiteering of the environment. Therefore, it is very important to monitor and recognize the changing trends of LULC, especially under the influence of urban variables and their brunt on the local landscape. Notable to the aliment and integration of ecosystems, as well as to environmental sustainability. Transition potential modeling uses different machine learning algorithms such as ANN-Multi layer perceptron, weights of evidence, multi-criteria evaluation, and logistic regression. It predicts possible changes in LULC under the influence of geographic variables and destinations to identify the location that causes changes. Most of these models use temporal land-use data to study land use land cover succession. Cellular automata simulate the ANN-MLP function in each

2. MATERIALS AND METHODS

2.1 Data Collection

Satellite images are available as direct JPG images and TIF raster data. The satellite images are downloaded from SENTINEL HUB. The other land scenes of images such as agricultural lands, roadways, and many more classes are acquired from the UC Merced land use dataset. The Raster form of LANDSAT-8 data is collected from Google Earth Engine. The data collected from the Earth engine is a compressed yearly record of 2017, 2020, and 2021 with a resolution of 30m. The geospatial variables such as city boundaries, road maps, river lines, water bodies, and elevation are obtained from DIVA-GIS. The precipitation data of India has been collected from CHRS DATA PORTAL for the last 20 years. The shape files are given appropriatecolor codes to differentiate in metrics.

2.2 Splitting of Data

The images are acquired and loaded. There are around 21 classes of scenes on land such as runways, parking lots, airplanes,forests, buildings, and beaches with each class containing 500 images. Out of 500, they are separated into training, testing, and validation sets. The training set contains 350 images, the testing set contains 50 images, and the validation set contains 100 images in every 21 classes. The ratios are 0.7, 0.1, and 0.2 respectively.

2.3 Convolutional Neural Network

There are separate libraries in machine learning to carry out the process of model building. The image data generator performs the scaler transformation of images from the input on a random basis. The layers of the model

are added successively to the existing layer to generalize the process effectively cell of the image. The results can be combined with geographic features to predict impending LULC whereabouts.We organized our research with clear-cut objectives.

- Building a machine learning model that classifies and identifies edges of the land objects.
- Determining land coverage area of satellite images.
- Predicting the land deformation by examining the land cover of past years.

The seperableConv2D layer acts on each channel at the input. Single convolution is separated into more convolutionsto produce the output at the end. The number of filters is set to 32, 64, and 128 on each step. The kernel size is 3 for all filters. The batch Normalisation function applies a transform to maintain the mean and standard deviation as 0 and1 respectively. The dropout layer sets 0 as the input units randomly with a frequency of 0.5 at each step during the training period. Maxpool2D down samples the input along its dimensions as 2 which is the maximum value over the input window. The input gets Flattened and the batch size is left unaffected.

A dense layer interconnects every neuron so that it takes input from all other neurons. 'Relu' is the common activation function to solve the disappearing gradient issues. Adam is a well-known optimizer and many researchers claim that the true properties of AdaGrad and RMSProp algorithms are collectively found in Adam optimizer. The model is trained with 50 epochs to attain an accuracy of up to 80%.

2.4 Computer Vision

Gaussian blur is applied to the images. This function makes the image convolve with the Gaussian filter to remove high-frequency components. The Gaussian kernel standard deviation is set to 3. The 'cvtColor' function can convert the color spaces of an image. Here, the image is converted to a gray color from the originally present RGB color space. Then, the canny edge detection algorithm is used to define the edges and boundaries of the object present within the image.

The threshold values are of two kinds, the lower value is set to 30 and the higher value is set to 200. These values correspond with gradient intensities. The 'add Weighted' function adds the image and the pixel values together. The alpha is 1.5, the beta is -0.5 and the gamma is 0. The original value is multiplied by 1.5 (alpha) and the blurred image is multiplied by - 0.5 (beta). These two values along with 0 (gamma) summed and display an image with points in the image when the color change occurs. These points are joined continuously along the boundaries. The points are retrieved externally and all the boundary points are stored. These contours are referred to as signatures of the surface objects.

2.5 Masks

The original image of SENTINEL has a wide area to analyze since the range would be in kilometers. Accessing every object is a tedious task. However, the nature of the ground surrounding can be estimated by masking techniques. This approach can determine the number of land usage. Ground truth mask is typically made by outlining the regions of interest with specific notations to evaluate computer vision algorithms. One hot encoded mask is a

2.6 Study Area - Coimbatore

Coimbatore is one of the biggest cities in South India, located underneath the Western Ghats, in Tamilnadu, India. The metropolitan stretches from 11.0168° N to 76.9558° E covering almost 800 square kilometers. It is a densely populated city with 1.6 million people (as of 2011). The climate was classified as Koppen with tropical wet and dry climatic conditions. The annual rainfall is around 650mm. The mountains and hills decorate the borders from north to west and are fine sharpness. The contours are marked as individual representations of an image by a binary vector of the size corresponding to the numberof classes in the image. Each pixel assigned with a binary vector is represented with "1" in the position related to the class label and "0" in all other positions.

Other masks are made by converting them from RGB to HSV values. The green mask is made to identify vegetation and crop growth areas, the brown mask can identify barren lands and roads, the grey mask can be involved in detecting cloud cover over the region, and the white mask can detect snow cover. Combining all these four masks can form a developed image, where the lambda function rounds off the mask to varying mean. The percentage of each type of land can be calculated.

A reserve forest area. The river of Noyyal runs through the southern boundary. The city has eight major wetland areas, with home to 120 species of birds. The northern part has a rich tropical forest with commercially valuable trees. The soil is suitable for cotton cultivation which boosts the textile industries. Coimbatore houses more than 30,000 industries and is rightly known as the "Manchester of South India". The Gross domestic product (GDP) is 45 billion dollars in 2021. The geographical location of Coimbatore is shown in Figure-1.

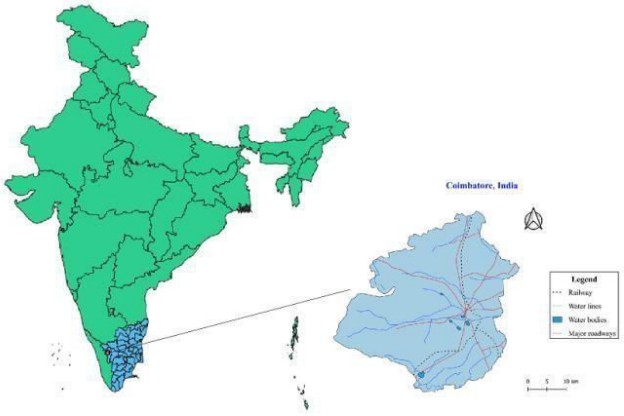

Figure-1. Geographical location of Coimbatore in India.

2.7 SCP

The data from the LANDSAT-8 satellite is processed from the Google Earth engine. The band combinations are set to 5-4-3.The raster data is clipped to our study area. Rather than obtaining land cover data from external resources, our research aims to build our land cover map by aiding the Semi- automatic classification plugin in QGIS. The process begins with creating numerous polygons to cover the regions of built-ups, water bodies, dark vegetation, and vegetation lands.

These polygons are known as signatures which act as training inputs. Totally 4 main classes with each main class contributingto several sub-classes. Each main class is represented with different colors. The spectral signatures are plotted on a graph. The classification tool of the SCP uses the trained signature file to convert the raster data to a simple land cover map. Two land cover maps of 2017 and 2020 are processed using SCP.

2.8 Normalized Indices

Now, from the raster data, the normalized indices of vegetation, water, and built-up are projected using the raster calculator. The formula for Normalized difference vegetation index (NDVI), Normalized difference water index (NDWI), and Normalized difference built-up index (NDBI) are,

NDVI = (Band 5 – Band 4) / (Band 5 + Band 4)
NDWI = (Band 3 – Band 5) / (Band 3 + Band 5)
NDBI = (Band 6 – Band 5) / (Band 6 + Band 5)

2.9 MOLUSCE

Modules for land use change evaluation is a powerful tool for analyzing and modeling land use changes. It simulates the interactions between the land covers and classes such as vegetation and urban areas. The inputs are raster data such as landcover of 2017 (initial) and landcover of 2020 (final) with spatial variables (Figure-2) such as elevation, distance from water and roads, and precipitation vector of the year 2017. The correlations are evaluated for all raster combinations. Pearson's correlation is a statistical measure that is used to determine the direction and strength of the two variables and establish a linear relationship, yet some data are randomly distributed. It ranges from -1 to 1. The correlation for both land covers is identified.

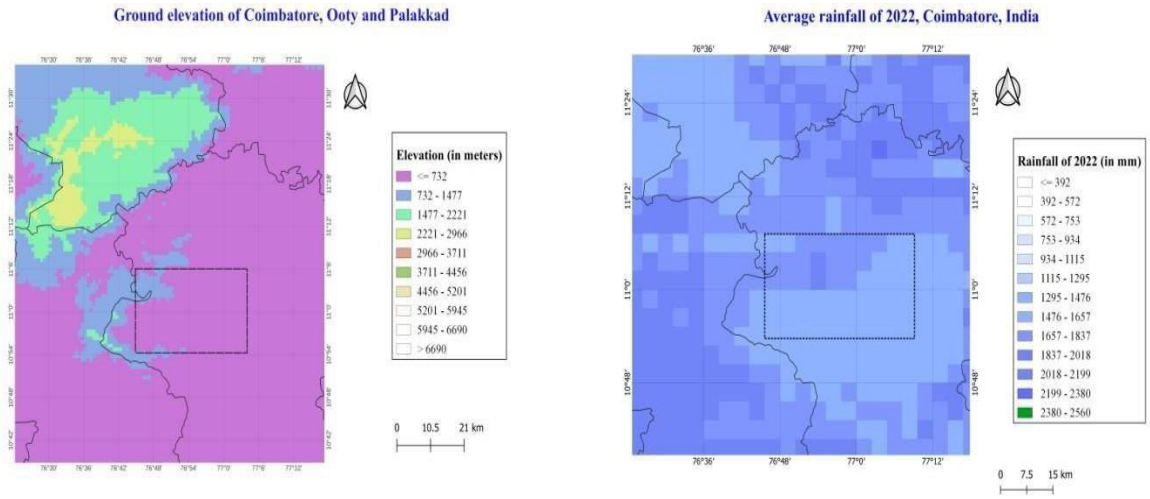

Figure-2. The elevation map is on the left side and the annual rainfall map is on the right side.

The area changes are neatly obtained from the pixels. Each pixel is 1x1 in dimension and the possible color changes happen pixel by pixel allowing the plugin to identify the area in raster units and square kilometers. The total land usage is now differentiated into 4 classes each possessing its allowed percentages. The rate of change from 2017 to 2020 is also claimed. The transition matrix shows the probabilities of moving from one class to another class. For example, the vegetation land in 2017 can be changed into built-up in 2020. Similarly, all the changes are obtained in the matrix. A changes map is createdusing these values.

The change map is subjected to transition potential modeling. The algorithm of Multi-layer perceptron is chosen for the learning phase. It is a feed forward neural network that has multiple layers of

perceptrons. They are interconnected by input and output layers. In this learning process, the neighborhood value of 1x1 pixel, the learning rate of 0.1000, the number of hidden layers as 10, and momentum as 0.050 with iterations as 1000 are chosen. After the learning phase, the process of cellular automata simulation is carried out with 2iterations for better results.

The landcover map of 2023 is produced and this predicted or deformed land cover is compared with the most recent landcover in 2020. The validation iterations are set to count 5. The plot of the multiple- resolution budget is prepared. The overall kappa coefficient achieved is 0.80. Similarly, with the predicted map of 2023, the land cover of 2026 can be determined. The reference land covers had 3 years in difference so that the predicted land cover will project the data from the next three years. The overall kappa coefficient for land cover in 2026 is 0.89.

2.10 Mapping

The obtained land covers and land cover changes from QGIS are mapped with layouts consisting of coordinate reference systems (CRS) and legends to identify changes.

3. RESULTS

3.1 Drawing Edges and Contours

The Canny edge detector algorithm and find Contour function develop the surfaces referring to the properties of the objects present in the image. The fine edges are drawn with grayscale images and added weights from the Gaussian blur are shown in the Figure-4.

3.2 Sequential Model

The image data generator is used to train the input samples, with a shear range of 0.3, and brightness ranges from 0.2 to 0.9. The layer stack of the model is shown. With Adam optimizer being evident, the 'categorical cross entropy' is a loss function for our model which calculates the difference between the predicted probabilities and true distribution of the model. The values indicate a better model fit. The plot is drawn with the values of accuracy, loss, validation accuracy, and validation loss for 20 epochs as shown in Figure-5.

3.3 Masks

The original satellite image can be studied from various points of view. The results (Figure-6) of the Ground truth mask and one hot encoded mask signify the land coverage of the locality. The pixels and saturation content of the ground data are unchanged; it just adds a layer to our examination.

Fine-tuning the levels of HSV standards can develop green, brown, white, and grey masks. The percentage of land coverage can be determined from the total developed image as in Figure-7.

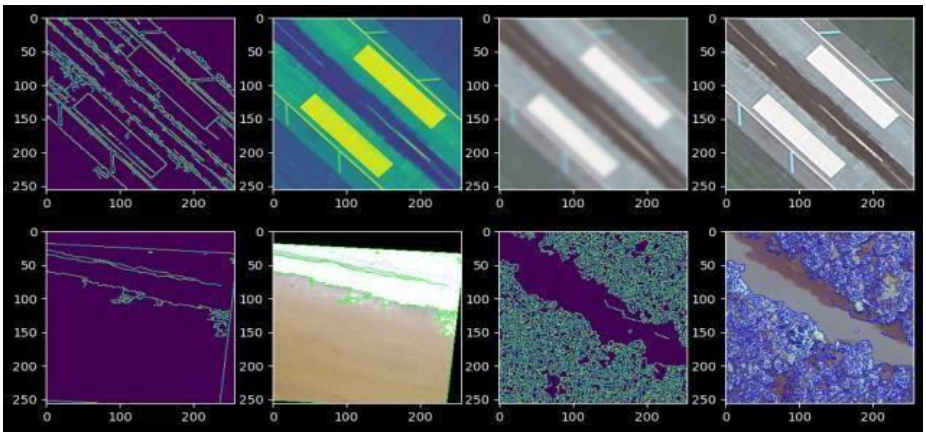

Figure-4. Edge detection with sharpness, and contour.

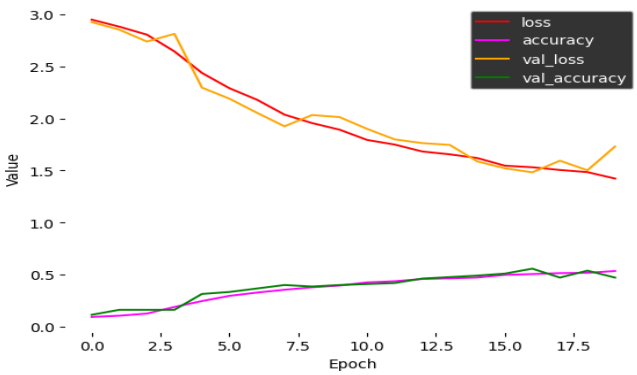

Figure-5. Epochs Vs values of metrics.

Figure-6. Ground truth and one hot encoded mask.

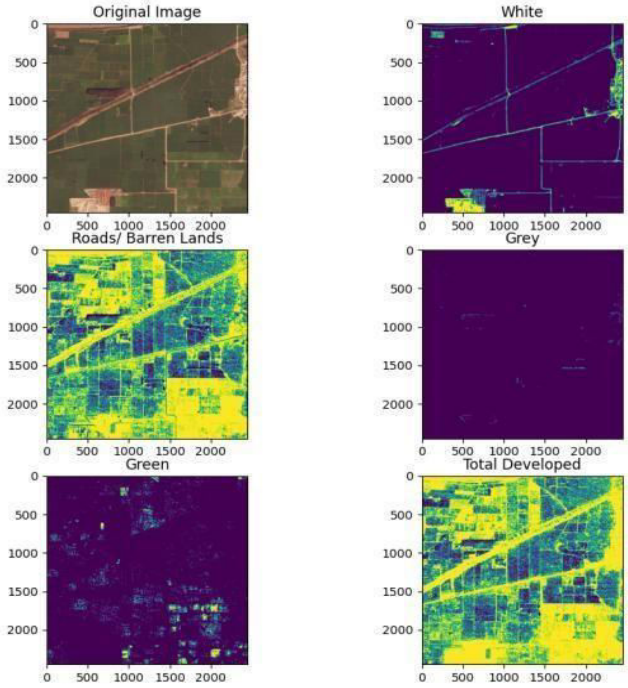

Figure-7. HSV altered masks.

3.4 Signatures in SCP

The ROIs are created over the raster map. They are denoted as spectral signatures and their plot between spectral valuesVs wavelength is shown in Figure-8.

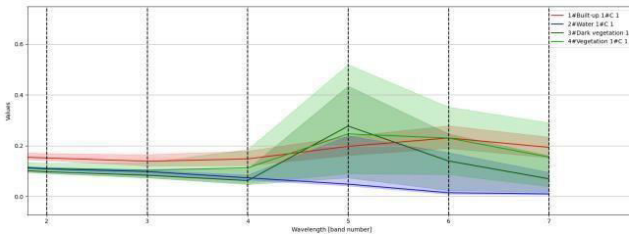

Figure-8. Spectral signatures of 4 classes.

A scatter plot of 4 distinct classes at bands 1 and 2 is shown in Figure 9.

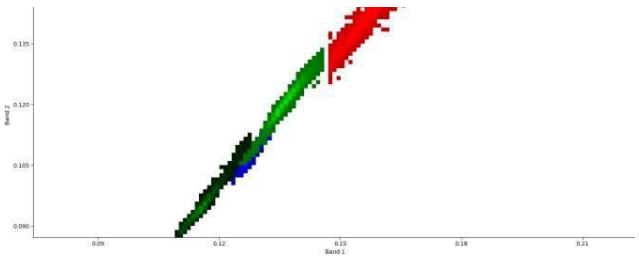

Figure-9. Scatter plot of spectral signatures.

The normalized indices of vegetation, water, and built-up are visualized with the help of a raster calculator in the QGIS toolbar as in Figure-10.

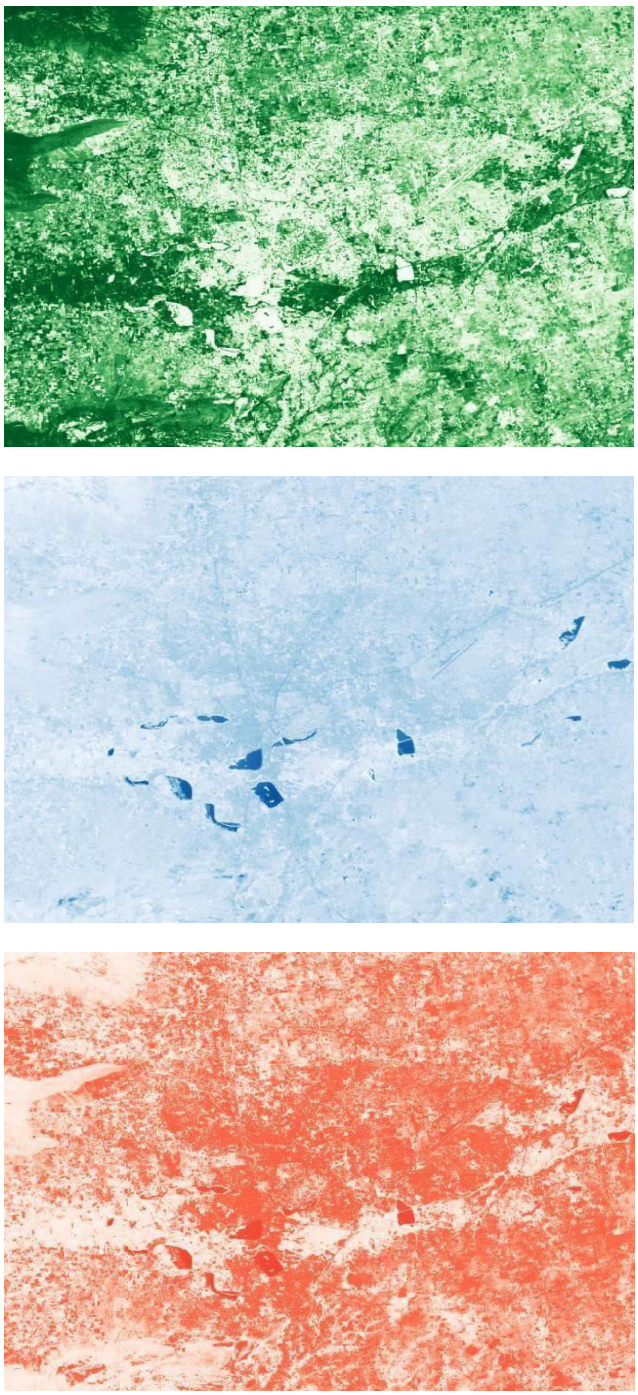

Figure-10. The normalized indices of vegetation (NDVI), water (NDWI), and built-up (NDBI).

3.5 Landcover Maps

The created land cover maps for the years 2017 and2020 are shown in Figure-11. These two maps are taken as input in the MOLUSCE plugin, with variable vectors such as elevation, and precipitation. The feature mapsof the Coimbatore district are shown in Figure-2.

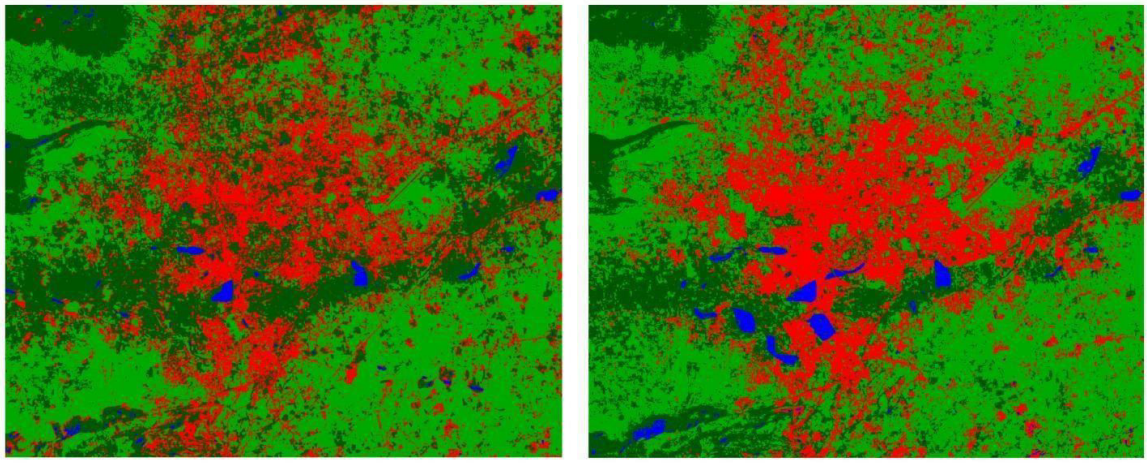

Figure-11. Created land cover map using SCP.

3.6 Changes in Area

The prediction of land cover in 2023 requires the land cover data for 2017 and 2020. The changes caused by built-up, water, and vegetation are noted. The Built- up area in 2017 was 165.68 sq. km and in 2020 it increased to 180.50 sq. km with a difference of 14.82 sq. km in three years. The area covered by water bodies in 2017 is 6.05 sq. km and in 2020 it increased to 10.55 sq. km with a difference of 4.50 sq. Km. Most of the dark vegetation lands such as forests are reduced from 224.35 sq. km to 161.46 sq. km. They were replaced by usual vegetation lands such as agricultural lands and some barren lands from 324.25 sq. km to 367.81 sq. km.

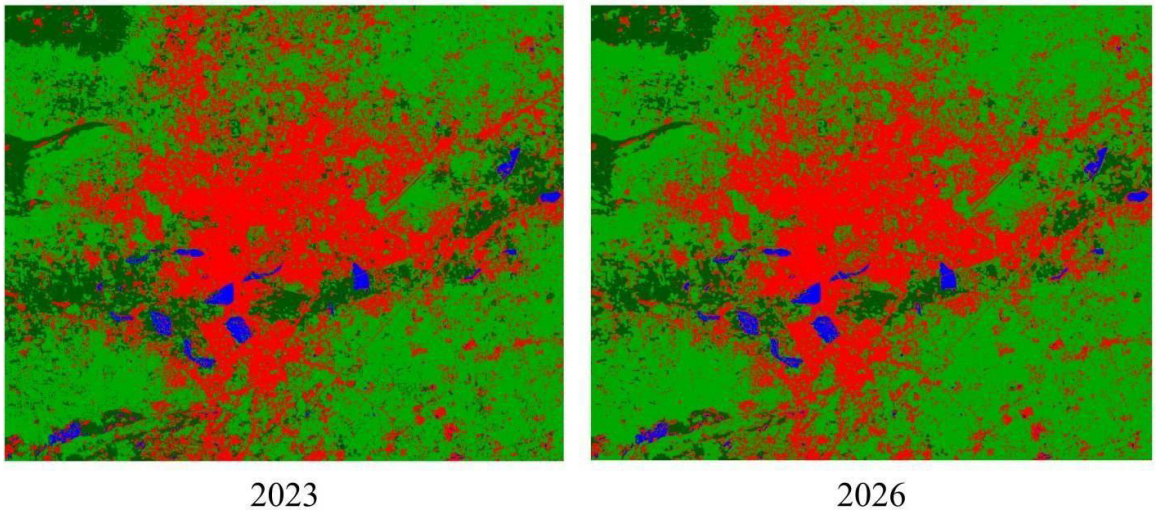

Figure-12. Predicted land cover map using MOLUSCE.

The overall statistics and transition matrix are shown. Now, the prediction of land cover in 2026 can be done by the land cover of 2020 and the predicted land cover of 2023 as in Figure-12. The built-up area was increased to 228.70 sq. km with a difference of 48.20 sq. km with a comparison to 2020. The water bodies are reduced to 9.01 sq. km and dark vegetation sinks further to 102.62 sq. km. Though the vegetation and barren lands have raised to 380.00 sq. km contributing to 52.75% of total land cover in 2023. The transition matrix identifies the changes within the classes with probabilities. The statistics ofall changes and the transition map are shown in Tables 1 to 3 and 5 to 7.

Table-1. Land area changes from 2017 to 2020.

	Class	2017	2020	Δ	2017%	2020%	Δ%
1	Build-up	165.68 sq. km	180.50 sq. km	14.82 sq. km	23.000	25.057	2.057
2	Water	6.05 sq. km	10.55 sq. km	4.50 sq. km	0.839	1.464	0.625
3	Dark vegetation	224.35 sq. km	161.46 sq. km	-62.88 sq. km	31.145	22.415	-8.729
4	Vegetation	324.25 sq. km	367.81 sq. km	43.56 sq. km	45.014	51.061	6.047

Table-2. Land area changes from 2020 to 2023.

	Class	2020	2023	Δ	2020%	2023%	Δ%
1	Build-up	180.50 sq. km	228.70 sq. km	48.20 sq. km	25.057	31.749	6.691
2	Water	10.55 sq. km	9.01 sq. km	-1.55 sq. km	1.464	1.250	-0.214
3	Dark vegetation	161.46 sq. km	102.62 sq. km	-58.85 sq. km	22.415	14.245	-8.169
4	Vegetation	367.81 sq. km	380.00 sq. km	12.20 sq. km	51.061	52.754	1.692

Table-3. Land area changes from 2023 to 2026.

	Class	2023	2026	Δ	2023%	2026%	Δ%
1	Build-up	228.70 sq. km	233.38 sq. km	4.68 sq. km	31.749	32.398	0.649
2	Water	9.01 sq. km	8.89 sq. km	-0.11 sq. km	1.250	1.234	-0.015
3	Dark vegetation	102.62 sq. km	64.87 sq. km	-37.35 sq. km	14.245	9.005	-5.240
4	Vegetation	380.00 sq. km	413.18 sq. km	33.18 sq. km	52.754	57.361	4.606

Table-4. Reference table for transition matrix.

S. No	Terrain distribution
1	Built-up, industries, and construction buildings
2	Water, lakes, and ponds
3	Dark vegetation, forest
4	Vegetation, agricultural and barren lands

Table-5. Transition matrix from 2017 to 2020.

Year	2020				
2017	Class	1	2	3	4
	1	0.619	0.007	0.075	0.298
	2	0.049	0.694	0.210	0.044
	3	0.131	0.014	0.581	0.271
	4	0.148	0.005	0.053	0.793

Table-6. Transition matrix from 2020 to 2023

Year	2023				
2020	Class	1	2	3	4
	1	0.967	0.000	0.000	0.031
	2	0.089	0.853	0.001	0.055
	3	0.210	0.000	0.633	0.156
	4	0.052	0.000	0.000	0.947

Table-7. Transition matrix from 2023 to 2026.

Year	2026				
2023	Class	1	2	3	4
	1	0.966	0.000	0.000	0.033
	2	0.008	0.987	0.000	0.003
	3	0.113	0.000	0.632	0.254
	4	0.001	0.000	0.000	0.998

3.7 Neural Network Learning

In the process of transition potential modeling, the learning curve of our neural network of algorithm Multi-layer perceptron is plotted as shown in Figure-13. The plot is drawn respective to the total number of iterations with overall accuracy and error. The current validation kappa is 0.55 for the land cover prediction of 2023 and 0.80 for the land cover prediction of 2026.

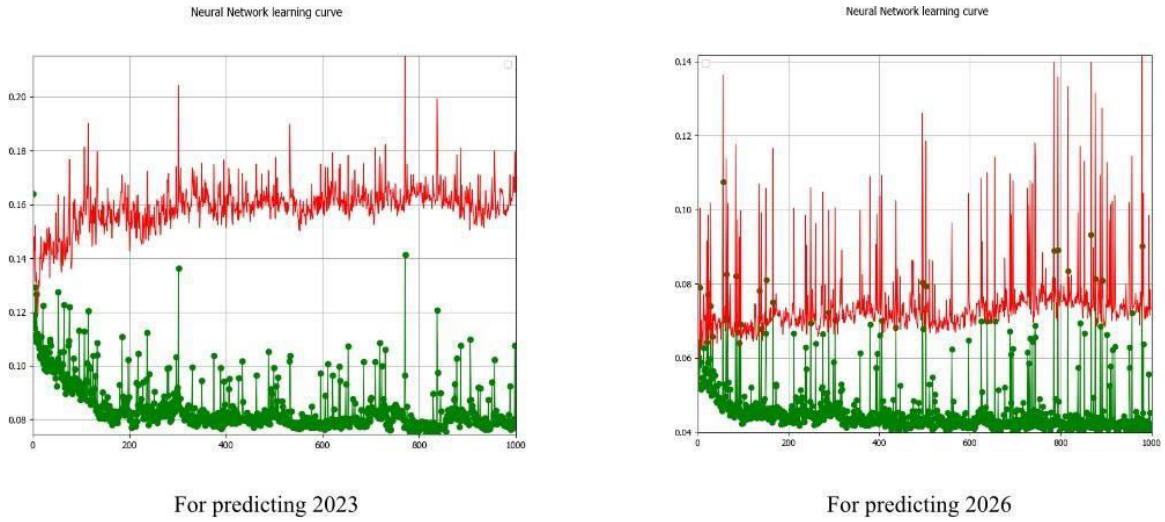

For predicting 2023 For predicting 2026

Figure-13. Learning curve of MLP.

3.8 Cellular Automata Simulation

The predicted results of land cover with the comparison with previous land cover data are shown in the figures. The built-up area is increased to 233.38 sq. km, the water area is decreased to 8.89 sq. km. With vegetation lands covering more than 57 percent of the total land distribution. Figure-14 shows the distribution changes from 2017 to 2026 with a span of 9 years.

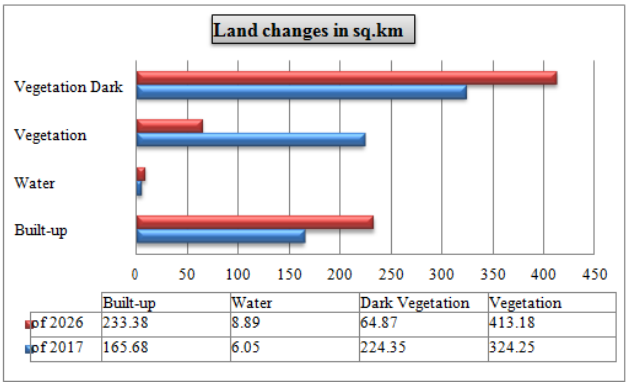

Figure-14. Predicted land changes from 2017 to 2026.

Table-8 shows the kappa coefficient calculation for the land covers 2017-20 and 2020-23.

Table-8. Kappa calculation.

Result	2017-2020	2020-2023
% Of Correctness	89.828	93.618
Kappa (overall)	0.837	0.890
Kappa (histo)	0.9266	0.909
Kappa (loc)	0.903	0.978

3.9 Changes Map

The changes map is made from the SCP toolbox, where the changes from the previous to present data are specified with different spectral values. These changes indicate areas where one class in the previous year is changed to a different class in the present year. These changes were made for 2020- 2023 and 2023-2026 land covers as shown in Figure-15. The bar plot is made to study the area distribution over the years as shown in Figure-16.

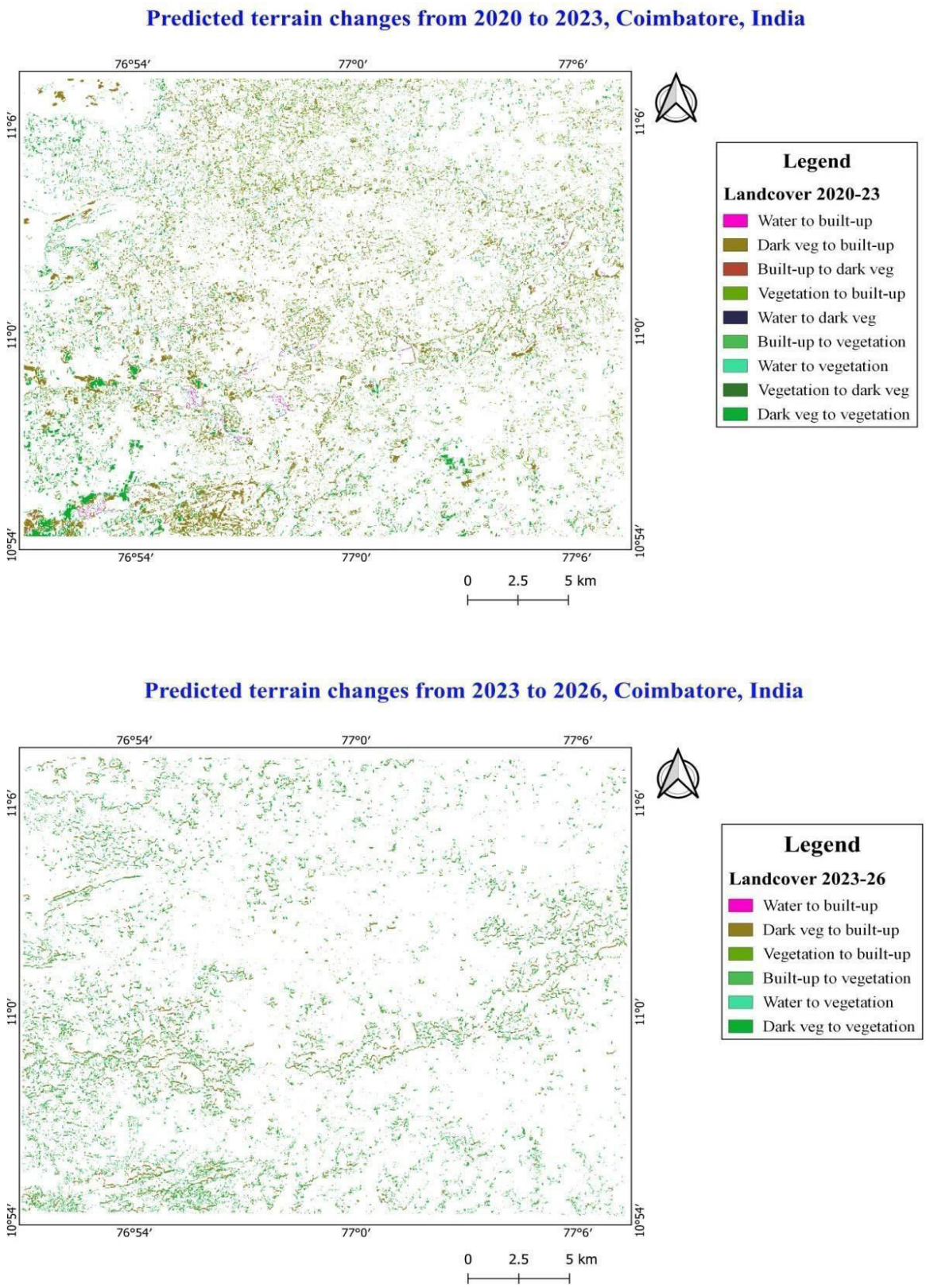

Figure-15. Changes map from the predicted land covers.

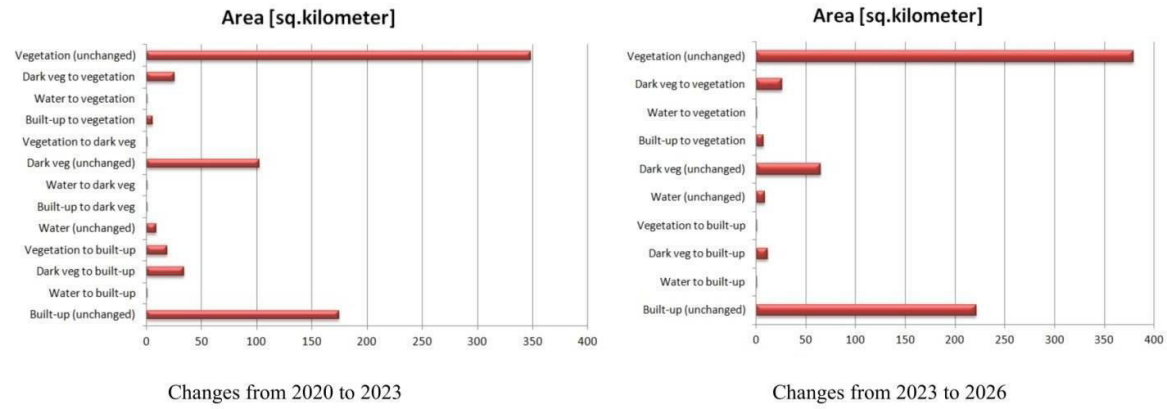

Figure-16. Bar plot indicating changes in the land distribution.

4. CONCLUSIONS

The findings of this research suggest that the factors are improper rainfall, distance from water lines to the cities, distance from road line to the vegetation lands, dense population, ground elevation, urbanization, and industrialization of Coimbatore has caused a noticeable impact on the land cover changes. Deforestation in the dark vegetation area has not only affected the local habitats but also the wildlife. The barren lands are taken down and more industries are being constructed causing a collapse in environmental sustainability. The downfall of water resources due to global warming poses a great threat. From our research, the predicted land deformation can be useful in determining governmental funds and policies before civilians are affected. Linking various policies and plans can integrate the action and bring a connected habitat.

REFERENCES

[1] M. Kanthi, T. H. Sarma and C. S. Bindu. 2020. A 3d-Deep CNN Based Feature Extraction and Hyperspectral Image Classification. 2020 IEEE India Geoscience and Remote Sensing Symposium (InGARSS), Ahmedabad, India.

[2] J. M. Bioucas-Dias, A. Plaza, G. Camps-Valls, P. Scheunders, N. Nasrabadi and J. Chanussot. 2013. Hyperspectral remote sensing data analysis and future challenges. IEEE Geoscience and Remote Sensing magazine. 1(2).

[3] H. -C. Shin *et al*. 2016. Deep Convolutional Neural Networks for Computer-Aided Detection: CNN Architectures, Dataset Characteristics and Transfer Learning. in IEEE Transactions on Medical Imaging. 35(51).

[4] Z. Tianyu, M. Zhenjiang and Z. Jianhu. 2018. Combining CNN with Hand-Crafted Features for Image Classification. 2018 14th IEEE International Conference on Signal Processing (ICSP), Beijing, China.

[5] B. Zhang. 2010. Computer vision vs. human vision. 9th IEEE International Conference on Cognitive Informatics (ICCI'10), Beijing, China.

[6] C. Akinlar and E. Chome. 2015. Canny S. R.: Using smart routing of edge drawing to convert Canny binary edge maps toedge segments. 2015 International Symposium on Innovations in Intelligent Systems and Applications (INISTA), Madrid, Spain.

[7] L. Yuan and X. Xu. 2015. Adaptive Image Edge Detection Algorithm Based on Canny Operator. 2015 4th International Conference on Advanced Information Technology and Sensor Application (AITS), Harbin, China. L. Wang and Y. Sun. 2021. Improved canny edge detection algorithm. 2021 2nd International Conference on Computer Science and Management Technology (ICCSMT), Shanghai, China.

[8] Soo-Chang Pei and Ching-Min Cheng. 1999. Color image processing by using binary quaternion-moment-preserving thresholding technique. in IEEE Transactions on Image Processing. 8(5).

[9] X. Deng, Y. Huang, S. Feng and C. Wang. 2010. Adaptive threshold discriminating algorithm for remote sensing image corner detection. 2010 3rdInternational Congress on Image and Signal Processing, Yantai, China.

[10] C. Bhuvan, S. Bansal, R. Gupta and A. Bhan. 2020. Computer Based Diagnosis of Malaria in Thin Blood Smears Using Thresholding Based Approach. 2020 7th International Conference on Signal Processing and Integrated Networks (SPIN), Noida, India.

[11] S. K. Chari, A. Gupta, P. Gupta and J. Mohan. 2017. Threshold selection in image segmentation using parametric entropy measures. 2017 Fourth International Conference on Image Information Processing (ICIIP), Shimla, India.

[12] K. Lowell, S. Reddy and E. Farmer. 2014. Data and sampling issues associated with accuracy assessment of landcover change maps produced from multi-temporal image classification. 2014 IEEE Geoscience and Remote Sensing Symposium, Quebec City, QC, Canada.

[13] M. N. Tapia and M. V. B. Morais. 2020. Land Use Data In The Middle Maule River Sub-Basin: Classification And Comparison Between 1999 And 2019. 2020 IEEE Latin American GRSS & ISPRS Remote Sensing Conference (LAGIRS), Santiago, Chile.

[14] N. M. Noor and A. Abdullah. 2015. Sustainable urban planning mapping using remote sensing and GIS in Malaysia. 2015 Joint Urban Remote Sensing Event (JURSE), Lausanne, Switzerland.

[15] S. Sim. 2007. Spatio-temporal dynamics in Seoul Metropolitan Region: Linking remote sensing into urban theory. 2007 Urban Remote Sensing Joint Event, Paris, France.

[16] Y. He, E. Lee and T. A. Warner. 2016. Continuous annual land use and land cover mapping using AVHRR GIMMS NDVI3g and MODIS MCD12Q1 datasets over China from 1982 to 2012. 2016 IEEE International Geoscience and Remote Sensing Symposium (IGARSS), Beijing, China.

[17] B. Seo, C. Bogner, T. Koellner and B. Reineking. 2016. Mapping Fractional Land Use and Land Cover in a Monsoon Region: The Effects of Data Processing Options. in IEEE Journal of Selected Topics in Applied Earth Observations and Remote Sensing. 9(9).

[18] D. R. Sowmya, V. S. Hegde, J. Suhas, R. V. Hegdekatte, P. D. Shenoy and K. R. Venugopal. 2017. Land Use/ Land Cover Classification of Google Earth Imagery. 2017 IEEE International WIE Conference on Electrical and Computer Engineering (WIECON-ECE), Dehradun, India.

[19] Aixia Chen, Yuanyuan Shen and Chuan Chen. 2010. Astudy on the area land use/land cover change and driving mechanisms applying RS/GIS. 2010 International Conference on Mechanic Automation and Control Engineering, Wuhan, China.